Article

Journal of the Brazilian Chemical Society

https://dx.doi.org/10.21577/0103-5053.20230191

J. Braz. Chem. Soc. **2024**, *35*, 6, e-20230191, 1-11

Electrochemical Investigations of Protein Denaturating Agents Dithiobutylamine and Dithiothreitol and of the Antineoplastic Alemtuzumab at Glassy Carbon Electrode

Nathalia L. Queiroz,[a] Maycom W. F. Silva,[a] Maysa L. Nascimento,[a] José G. da Silva Neto,[a] José Ailton M. Nascimento,[a] Katia C. S. Freitas,[a] Eric S. Gil[b] and Severino Carlos B. Oliveira[*,a]

[a]Departamento de Química, Universidade Federal Rural de Pernambuco, 52171-900 Recife-PE, Brazil

[b]Faculdade de Farmácia, Universidade Federal de Goiás, 74605-170 Goiânia-GO, Brazil

A study to establish redox and thermodynamic properties of the protein denaturing agents dithiobutylamine (DTBA) and dithiothreitol (DTT) and of the monoclonal antibody alemtuzumab (ATZ), in aqueous electrolytes, with different pH values, under different experimental conditions, was carried out on a glassy carbon electrode (GCE), using cyclic voltammetry (CV), differential pulse voltammetry (DPV) and square wave voltammetry (SWV). The voltammetric study demonstrated that DTBA, as well as DTT, were both susceptible to direct electro-oxidation on the electrode surface. The study established that the oxidation of DTBA and DTT took place in three subsequent steps, the first two occurring in the thiol groups forming a cyclic intermediate. The oxidation mechanisms of DTBA and DTT were postulated and proposed. The results using DPV and SWV clearly demonstrated the spontaneous adsorption of ATZ on the hydrophobic GCE surface and that it undergoes electro-oxidation in amino acid residues of tyrosine and tryptophan, exposed superficially on the three-dimensional structure of the protein and on the electrode. An oxidation mechanism of ATZ was also proposed.

Keywords: protein denaturing agents, dithiobutylamine, dithiothreitol, cysteine, alemtuzumab

Introduction

About 20% of proteins have disulfide bonds between cysteine residues (Cys),[1-4] Scheme 1. The oxidation state of thiol groups (RSH) is determinant in the structure and consequently in the activity of physiological processes, since the reaction exchange rate RSH/RSSR is important in protein folding, enzymatic catalysis and even deoxyribonucleic acid (DNA) cleavage.[1-4] Small molecules that have thiol groups, Scheme 1, are widely used as reducing agents in biochemical methodologies for characterization, detection and quantification of biomolecules, with the main aim of reducing disulfide bonds, for example, by facilitating the denaturation of proteins.[1-4]

Beta-mercaptoethanol (β-ME) used to be the most common agent to reduce disulfides of biomolecules.[3,4] With the thiol group of pK_a = 9.61, in neutral medium, however, it had a very slow reaction kinetics and was trapped in the reduced species.[3,4] Dunaway-Mariano *et al.*[4] comprehended that a dithiol would solve these problems and proposed the racemic (2*S*,3*S*)-1,4-dimercaptobutane-2,3-diol (dithiothreitol or DTT), Scheme 1, with two thiol groups with pK_a values of 9.2 and 10.1.[3] The reaction kinetics of DTT were faster compared to β-ME and the reaction product was cyclic and easily separated.[3,4] However, DTT as a reductant still had reaction kinetics at neutral pH considered slow, since its reactivity is driven by thiolate anions.[1,5] Aiming at faster reaction kinetics, Lukesh *et al.*[1]

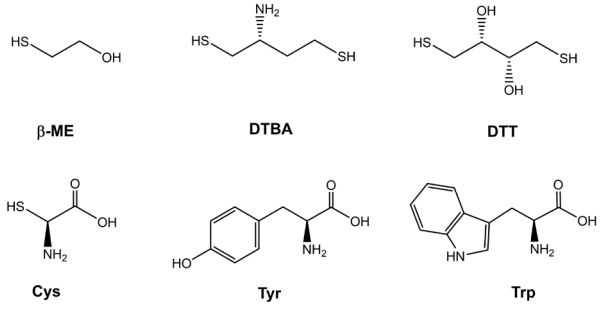

Scheme 1. Chemical structures of the reducing agents, beta-mercaptoethanol, dithiobutylamine and dithiothreitol and of the amino acids cysteine, tyrosine and tryptophan.

*e-mail: s.carlosb.oliveira@gmail.com; severino.oliveira@ufrpe.br
Editor handled this article: Rodrigo A. A. Muñoz (Associate)

synthesized dithiobutylamine (DTBA), Scheme 1, a no racemic dithiol with pK_a values of 8.2 and 9.3. At a neutral pH, DTBA reduces disulfides faster than DTT.[1,6] In addition, it is more efficient in restoring the enzymatic function of proteins[1,6] and has also been used as a ligand for various metal ions forming mono and dinuclear complexes.[6]

Advances in biotechnology have enabled the design and production of antibodies that target specific antigens, such as those found in cancer cells.[7] These antibodies are called monoclonal antibodies (mAbs).[7] The mAbs are formed by four polypeptide chains, two heavy and two light, connected mainly by disulfide bonds.[8,9] The mAbs have been increasingly used in the treatment of cancer, since they have a specific target, preserving normal cells and minimizing the side effects caused by traditional chemotherapy.[8,9]

Alemtuzumab (ATZ) is a mAb that has two identical heavy chains, with 451 amino acids each, and two identical light chains, with 211 amino acids each, with a molecular mass of 146 kDa.[10] In addition, they are used in the treatment of various types of autoimmune diseases such as rheumatoid arthritis,[11,12] vasculitis[13,14] and scleroderma.[15] ATZ has been widely used in cases of B-cell chronic lymphocytic leukemia, in patients who have not obtained a satisfactory response to chemotherapy with alkylating agents and therapy with fludarabine,[8,9,16] and also for the treatment of patients with active relapsing-remitting multiple sclerosis.[10,17-19]

Electrochemical studies with carbon electrodes have been decisive in the investigation of redox and thermodynamic properties of different chemical species,[20-24] of immobilization of macromolecules on surfaces,[24-26] as well as, on the development of sensors for different applications[27-29] and of analytical and bioanalytical methods.[22,23,27,28] Furthermore, the electrochemical behavior of electroactive amino acid residues, tyrosine (Tyr),[22,29,30] tryptophan (Trp),[31,32] cysteine (Cys),[33] Scheme 1, histidine (His)[22] and methionine (Met)[33] and proteins[24,25,29] have already been explored. These studies can be useful to clarify mechanisms related to redox stability, physiological and pharmacological activity.[20-32] However, to our knowledge, to date, no studies to establish the electrochemical properties of ATZ, as well as of the denaturing agent DTBA, have been reported in the literature. DTT anodic oxidation mechanism was investigated at glassy carbon electrode, but only under specific conditions and using differential pulse voltammetry (from 1.0 to 1.4 V *vs.* an Ag/AgCl reference electrode).[2] However, only one DTT oxidation peak was detected, and additional work needs to be done to fully characterize the electrochemical redox behavior of DTT.

The present work aimed to investigate, for the first time, the anodic behavior of DTBA, DTT and ATZ in aqueous supporting electrolytes, with different pH values, with a glassy carbon electrode (GCE), using voltammetric techniques, cyclic voltammetry (CV), differential pulse voltammetry (DPV) and square wave voltammetry (SWV). Furthermore, the voltammetric results of ATZ were compared with the electro-oxidation of the amino acids Trp and Tyr.

Experimental

Chemicals and reagents

Monoclonal anti-CD52 antibody 1 mg mL^{-1} ATZ in an aqueous phosphate buffer solution, pH = 7.4, was obtained from Sigma-Aldrich (St. Louis, USA) and stored at 4 °C.

DTBA, DTT, Trp, Tyr and Cys reagents were obtained from Sigma-Aldrich (St. Louis, USA) and used without further purification. Fresh stock solutions of 2 mmol L^{-1} DTBA and 2 mmol L^{-1} DTT were prepared in deionized water. Stock solutions of Tyr, Trp and Cys amino acids were prepared by weighing the solids, after they were dissolved with a few drops of 0.2 mol L^{-1} NaOH and diluted with the buffer solution to the desired volume. The concentrations used in the voltammetric tests were prepared by diluting the respective stock solutions in the aqueous supporting electrolyte solution, directly in the electrochemical cell. Aqueous supporting electrolyte solutions with different pH values were prepared using analytical grade reagents and deionized water.[22] To prepare the solutions, ultrapure water (conductivity < 0.1 μS cm^{-1}) from Millipore Milli-Q (Bedford, USA) was used.

The pH measurements were performed with a Metrohm Herisau pH-meter (Switzerland) using a Scott Gerate combination glass electrode. All experiments were carried out at room temperature, T = 25 ºC.

Voltammetric parameters and electrochemical cells

Electrochemical experiments were performed using a three-electrode potentiostat (PGSTAT 302N model, Metrohm, Netherlands) with NOVA 2.0 software (Metrohm/Autolab, Netherlands). The tests were based on a GCE with a diameter of 1.6 mm (ALS, Japan) or 3.0 mm (Metrohm, Brazil), a Pt wire auxiliary electrode and an Ag/AgCl (3 mol L^{-1} KCl) reference electrode, in a 10 mL electrochemical cell. The operating parameters for DPV were pulse amplitude of 50 mV, pulse width of 70 ms and sweep speed of 5 mV s^{-1}. For SWV, these parameters were pulse amplitude of 50 mV, frequency of 10 Hz and potential

increment of 5 mV, corresponding to an effective sweep speed of 50 mV s^{-1}. For the electrochemical impedance spectroscopy (EIS), the following parameters were used: root mean square disturbance (rms) of 5 mV, 10 frequency values *per* decade, with a frequency range from 65.000 to 0.01 Hz. All studies were carried out in triplicate.

Before starting each electrochemical test, the GCE was always polished with filter paper with diamond spray (particle size 1 µm, Kement, UK) and subsequently cleaned with deionized water. After this mechanical treatment, the GCE was placed in the electrochemical cell with adequate supporting electrolyte and an anodic pre-treatment was performed, where several successive voltammograms were repeatably recorded in a positive potential window, until the electrochemical response remained unchanged (baselines stable). This pre-test conditioning of the GCE surface ensured reproducible experimental results.

A thin film of ATZ on the GCE was prepared via spontaneous adsorption from a drop of 5 µL of the 1 mg mL^{-1} ATZ solution placed on the GCE surface and dried at room temperature for 10 min. Subsequently, the electrode was carefully washed with deionized water and placed in the electrochemical cell containing only the supporting electrolyte.

All DPVs presented in this work were submitted to the moving average mathematical method for baseline correction, using a potential step of 2 mV.

Results and Discussion

Electrochemical study of the reducing agents dithiobutylamine and dithiothreitol

The anodic behavior of DTBA on GCE, using voltammetric techniques, was investigated and compared with the electro-oxidation of DTT.

Consecutive cyclic voltammograms of 1.0 mmol L^{-1} DTBA in acid medium, pH = 4.5, detected three subsequent irreversible reactions: peak 1a at E_{p1a} = +0.23 V, peak 2a at E_{p2a} = +0.75 V and peak 3a at E_{p3a} = +1.37 V, Figure 1A and Table 1. As in the case of 1 mmol L^{-1} DTT, the voltammograms, under the same experimental conditions, detected four consecutive and irreversible anodic peaks: peak 1a at E_{p1a} = +0.23 V, peak 2a at E_{p2a} = +0.70 V, peak 2a' at $E_{p2a'}$ = +0.92 V and peak 3a at E_{p3a} = +1.32 V, Figure 1C and Table 1.

The above experiments were repeated in a physiological medium, at pH = 7.0. The cyclic voltammograms of

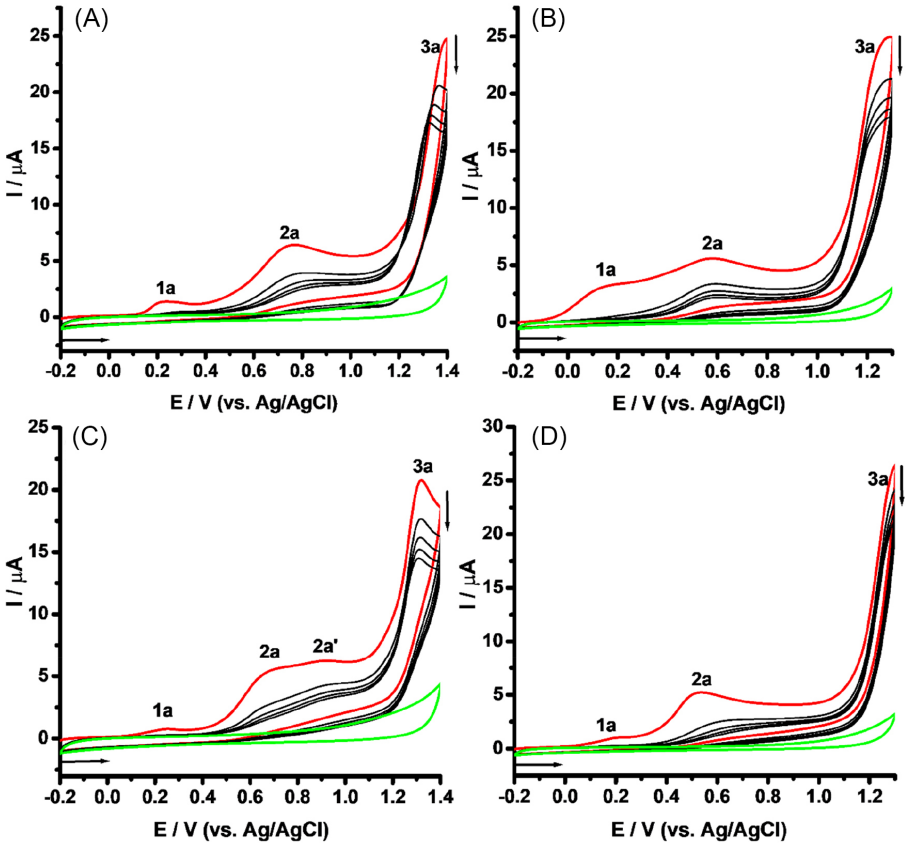

Figure 1. Consecutive cyclic voltammograms on GCE (1.6 mm) of 1 mmol L^{-1} DTBA (A and B) and of 1 mmol L^{-1} DTT (C and D); in acetate buffer at pH = 4.5 (A and C) and phosphate buffer at pH = 7.0 (B and D). First scan (—) and the supporting electrolyte (—), v = 100 mV s^{-1}.

Table 1. Peak potentials of DTBA and DTT in CV on GCE

Species	CV peak potentials (E / V *vs.* Ag/AgCl)							
	pH = 4.5				pH = 7.0			
	Peak 1a / V	Peak 2a / V	Peak 2a' / V	Peak 3a / V	Peak 1a / V	Peak 2a / V	Peak 2a' / V	Peak 3a / V
DTBA	+0.23	+0.75	–	+1.27	+0.15	+0.58	–	+1.28
DTT	+0.23	+0.70	+ 0.92	+1.32	+0.17	+0.53	–	+1.29

DTBA: dithiobutylamine; DTT: dithiothreitol; CV: cyclic voltammetry.

1 mmol L^{-1} DTBA showed three anodic peaks, all irreversible, at E_{p1a} = +0.15, E_{p2a} = +0.58 and E_{p3a} = +1.28 V, Figure 1B and Table 1. However, all processes when compared to the results at pH = 4.5, occurred at lower positive potential values, clearly demonstrating that these electro-oxidations were pH-dependent on the medium and occurred more easily, as expected, at neutral pH. The consecutive cyclic voltammograms of 1 mmol L^{-1} DTT showed an electrochemical behavior very similar to DTBA, with three subsequent irreversible anodic processes: E_{p1a} = +0.17, E_{p2a} = +0.53 and E_{p3a} = +1.29 V, Figure 1D and Table 1.

The results show, for both the acid and physiological media, that after the second cyclic voltammogram, Figure 1, there was a disappearance of the first oxidation process. There was also a very significant decrease in the currents of the subsequent peaks, 2a and 2a', due to the products of these electro-oxidations that strongly adsorb on the GCE surface.

To establish the mass transport of DTBA to the GCE surface, cyclic voltammograms with different scanning speeds, between 5 and 300 mV s^{-1}, were recorded in an aqueous solution of 1 mmol L^{-1} DTBA at pH = 7.0, Figure 2. After each scan, the electrode surface was always cleaned, to avoid problems resulting from the adsorption of DTBA oxidation products. The results showed that peak 2a currents had a linear relationship with the square root of the sweep speed, with correlation coefficient of 0.994, indicating that the DTBA mass transport to the electrode surface was predominantly diffusion controlled,[34,35] in agreement with the Randles-Sevcik equation for an irreversible system, equation 1.[22,34,35]

$$I_{pf} = 2.99 \times 10^5 n\,(\alpha_c + n')^{1/2} A C_0 D_O^{1/2} v^{1/2} \quad (1)$$

where I_{pf} is the peak current associated with the forward scan in Ampere, n is the number of electrons transferred during the oxidation of DTBA, α_c is the charge transfer coefficient, n' is the number of electrons in the rate-determining step, A is the GCE electroactive area in cm^2, D_O is the diffusion coefficient in $cm^2\ s^{-1}$, C_0 is the DTBA concentration in mol cm^{-3} and v is the scan rate in V s^{-1}.

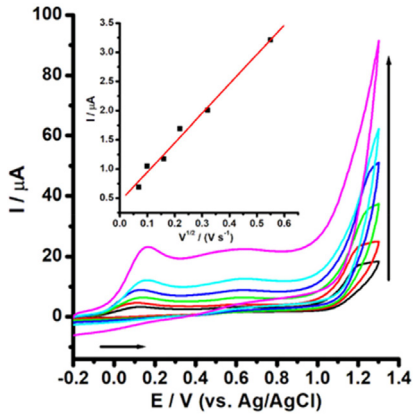

Figure 2. Cyclic voltammograms on GCE (3.0 mm) in solution of 1 mmol L^{-1} DTBA in phosphate buffer, pH = 7.0, under different scan rates, (—) 5, (—) 10, (—) 25, (—) 50, (—) 100 and (—) 300 mV s^{-1}. Inset: plot of I_{p1a} *vs.* $v^{1/2}$.

The Tafel plot and its corresponding slope were used for elucidating the oxidation mechanism of DTBA. The slope of the Tafel plot was equal to:

$$\text{Slope} = nF(1-\alpha)/2.3RT \quad (2)$$

where F is the Faraday constant in C, R is the universal gas constant in J K^{-1}, T is the temperature in K and n is the number of electrons involved in the redox process.[34,35] As the Tafel inclination was 4.29 V dec^{-1} with correlation coefficient (r) of = 0.998 and 3.46 V dec^{-1} with r = 0.999, for the anodic peaks 1a and 3a respectively, Figure 3, both processes occur therefore with a removal of one electron.

Cyclic voltammograms of Cys 1.0 mmol L^{-1} in neutral pH were recorded and compared to those of DTBA and DTT, Figure 4. Cys is an amino acid whose structure resembles the structure of DTBA and DTT; however, it has only a single thiol group in the side chain, Scheme 1.

In an acid medium, pH = 4.5, the Cys voltammograms, recorded in the potential window from E = –0.2 V to +1.45 V, detected two anodic peaks, at E_{pa} = +0.93 and at E_{pa} = +1.48,[33] Figure 4A. In the physiological medium, at pH = 7.0, the voltammograms recorded from E = –0.2 to +1.25 V, detected peaks at E_{pa} = +0.67 and at E_{pa} = 0.96 V,[33] Figure 4B.

Comparing the anodic behavior of Cys with that of

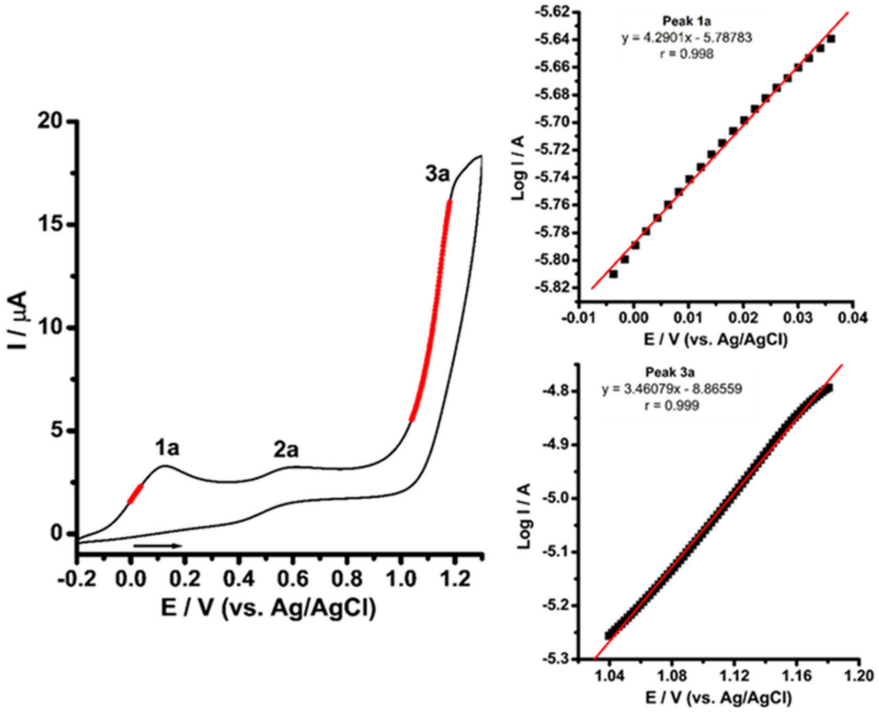

Figure 3. Cyclic voltammograms on GCE (3.0 mm) in solution of 1 mmol L^{-1} DTBA in phosphate buffer at pH = 7.0, v = 5 mV s^{-1} and the Tafel plot of the peaks 1a and 3a.

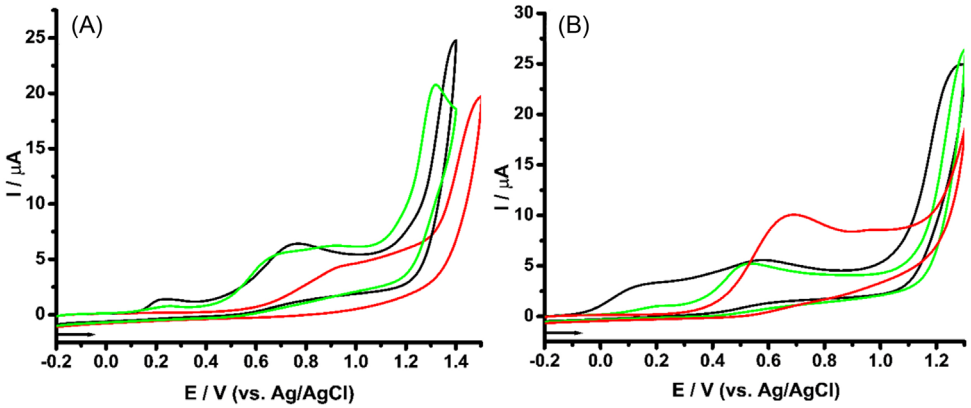

Figure 4. Cyclic voltammograms on GCE (1.6 mm) of 1.0 mmol L^{-1} Cys (—), DTBA (—) and DTT (—). (A) In acetate buffer, pH = 4.5 and (B) in phosphate buffer, pH = 7.0.

DTBA and DTT, Cys was not observed to be present in the first oxidation step, Figure 4. This is explained by the presence of only a single thiol group in its structure. Thus, the first and second anodic processes of DTBA and DTT were related to oxidations of existing thiol groups, Scheme 1.

The anodic behavior of DTBA and DTT were also investigated using SWV, in different aqueous electrolytes, Figure 5. Important advantages of SWV include high sensitivity, high peak resolution, minimization of problems with adsorption of products from subsequent steps on the electrode surface, high analytical frequency and electrochemical reversibility analysis of the electron transfer reaction requiring only a single potential scan.[34,35]

SWVs recorded in 1 mmol L^{-1} DTBA solutions prepared in acetate buffer, pH = 4.5 and in phosphate buffer, pH = 7.0, indicated data similar to those obtained by CV, showing three anodic peaks in the acid medium (E_{p1a} = 0.12, E_{p2a} = 0.65 and E_{p3a} = 1.32 V), Figure 5A, and in the physiological medium (E_{p1a} = 0.02, E_{p2a} = 0.50 and E_{p3a} = 1.17 V), Figure 5B. SWVs of DTT 1 mmol L^{-1} were performed under the same experimental conditions. In the acid medium, it was not possible to observe the first peak, peak 1a; only three oxidation peaks were detected (E_{p2a} = 0.58, $E_{p2a'}$ = 0.88 and E_{p3a} = 1.26 V), Figure 5C. In the physiological medium, three oxidation peaks were also detected (E_{p1a} = 0.02, E_{p2a} = 0.50 and E_{p3a} = 1.17 V), Figure 5D.

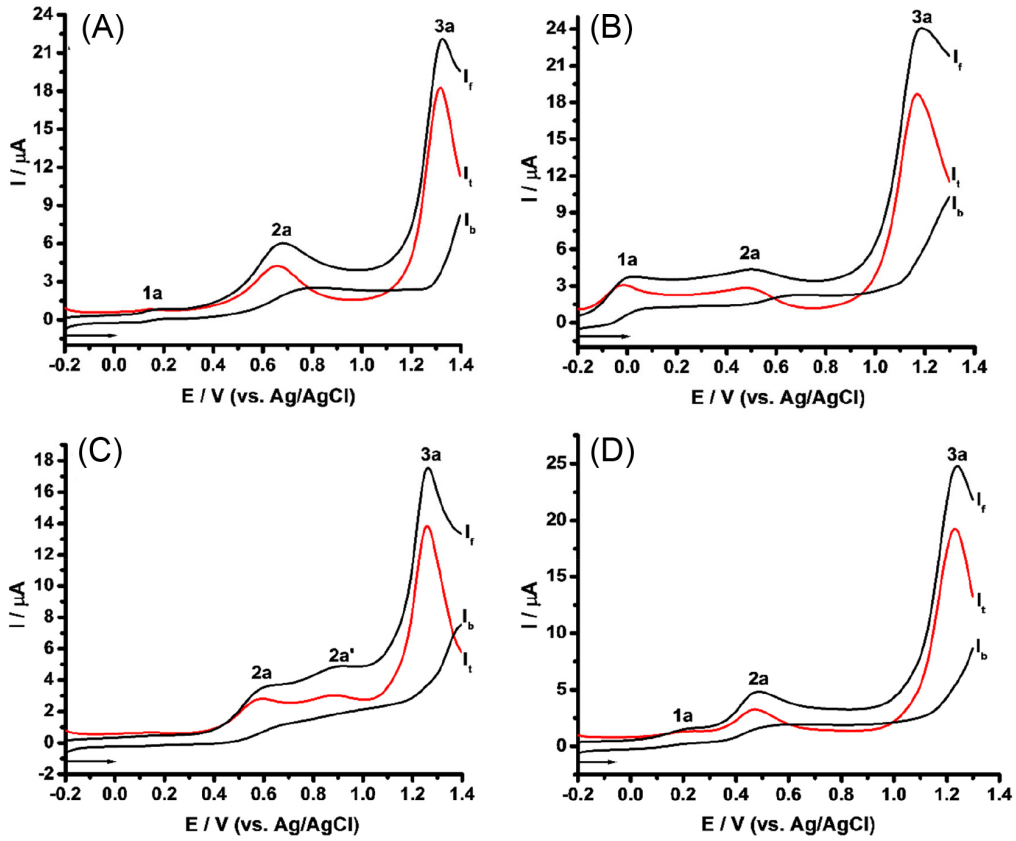

Figure 5. SWVs on GCE (1.6 mm) of 1 mmol L^{-1} DTBA (A and B) and of 1 mmol L^{-1} DTT (C and D) in (A and C) acetate buffer, at pH = 4.5 and (B and D) phosphate buffer, at pH = 7.0. I_f: forward, I_b: backward and I_t: total current voltammograms.

The SWV results indicated small differences in the anodic behavior of these agents, for example, for DTBA the peak 1a was identified in each investigated aqueous media, acidic and neutral, while for DTT this process was only detected in the physiological media. Yet, the anodic peak 2a' of DTT was only observed in acid media, Figure 5.

DPVs were also recorded in 1.0 mmol L^{-1} DTBA solutions prepared in aqueous supporting electrolytes with different pH values, Figure 6A. On the plot of peak potential as a function of pH, Figure 6B, a slope of –53 mV *per* pH unit shows that the mechanism associated with peak 1a involves an equivalent number of electrons and protons.[34,35] As from the DPV to the width of the peak at half height ($W_{1/2}$) (mV) = 90/n,[34,35] it can be concluded that this step of the reaction occurred with the removal of one electron and one proton. For peaks 2a and 3a, the inclinations were respectively –69 and –49 mV pH^{-1}; the DPV data indicates

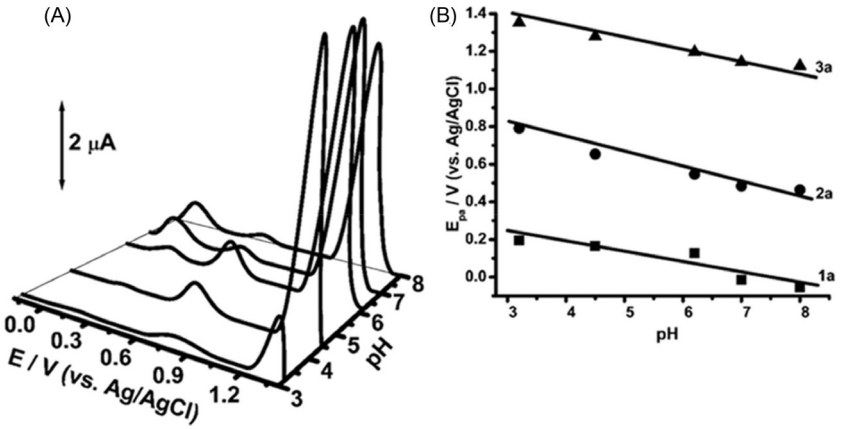

Figure 6. 3D plot of DPVs of (A) 1 mmol L^{-1} DTBA as a function of pH (3.5-8.0). (B) Plot of peak potential (■) 1a, (●) 2a and (▲) 3a as a function of pH.

that both processes occurred with the withdrawal of one electron/proton pair.[34,35]

The voltammetric results presented here are converging and indicate that DTBA, as well as DTT, undergo electro-oxidation on GCE in three subsequent steps and that they were associated with oxidation of the thiol groups of these molecules. The oxidation mechanisms of DTBA and DTT were postulated and proposed, Scheme 2, based on the voltammetric data, Figures 1-6, together with previous results from the literature.[33,36]

Scheme 2 proposes that the first two steps of dithiolic compounds, peaks 1a and 2a, refer to the electro-oxidations of the sulfydryl groups (–SH), for the formation of radicals that will react to form an intermediate cyclic product with a disulfide bond. The intermediate, referring to the first anodic process, is also adsorbed on the GCE and electro-oxidized in an aqueous medium at high potential values (peak 3a).[33,36] The electrochemical results presented here also indicated that DTBA and DTT were both oxidized at low potential values, therefore were indeed good reducing agents, unlike Cys. These electrochemical results are also complementary to the biochemical data,[1-6] further demonstrating the potential of DTBA as a protein reducing/denaturing agent.

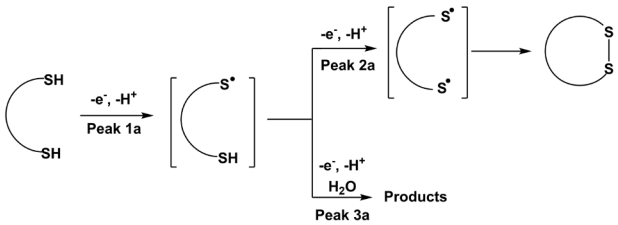

Scheme 2. Proposed oxidation mechanism of DTBA and DTT.

Electroanalytical determination of DTBA

DPV can be used for sensitive quantification of DTBA in phosphate buffer, pH = 7.0. Under optimized experimental conditions (pulse amplitude of 50 mV, pulse width of 70 ms and ν = 5 mV s^{-1}), voltammograms were recorded in solutions with different concentrations of DTBA and the variation in the current of the anodic peak 3a, referring to the oxidation of DTBA on the pre-treated GCE, was used as the analytical signal, Figure 7A.

The corresponding analytical curve, Figure 7B, proves that there is an excellent linear relationship, with the equation of the straight line I_{pa} (A) = 0.008(DTBA / (μmol L^{-1})) – 1.33 × 10^{-8}, with a coefficient of correlation 0.999, in the concentration range from 3.98-15.56 μmol L^{-1}. For each concentration, the electrode was always anodically pre-treated, and thoroughly rinsed with deionized water, in order to ensure a clean surface. The limit of detection (LOD) was 0.61 μmol L^{-1} (3σ/S, where σ is the standard deviation of the blank and S is the slope of the analytical curve) and the limit of quantification (LOQ) was 2.05 μmol L^{-1} (10 σ/S).

The repeatability of the proposed method (n = 4) was also investigated using a 6 μmol L^{-1} DTBA solution, Figure 7C. A relative standard deviation (RSD) of 6.7% was found, which demonstrated good measurement performance.

Electrochemical study of the anodic behavior of the monoclonal antibody alemtuzumab

The ATZ was immobilized on GCE by spontaneous adsorption (10 min). Its anodic behavior was then investigated in aqueous supporting electrolytes, Figure 8. Consecutive cyclic voltammograms of the ATZ thin film, recorded in the potential window from E = +0.40 to +1.30 V, showed two subsequent irreversible anodic peaks (E_{p1a} = 0.88 V, E_{p2a} = 1.18 V), in the first scan, Figure 8A. However, from the second potential scan, no redox process was identified, which is justifiable, since the ATZ amino acid residues exposed on the GCE were electro-oxidized.

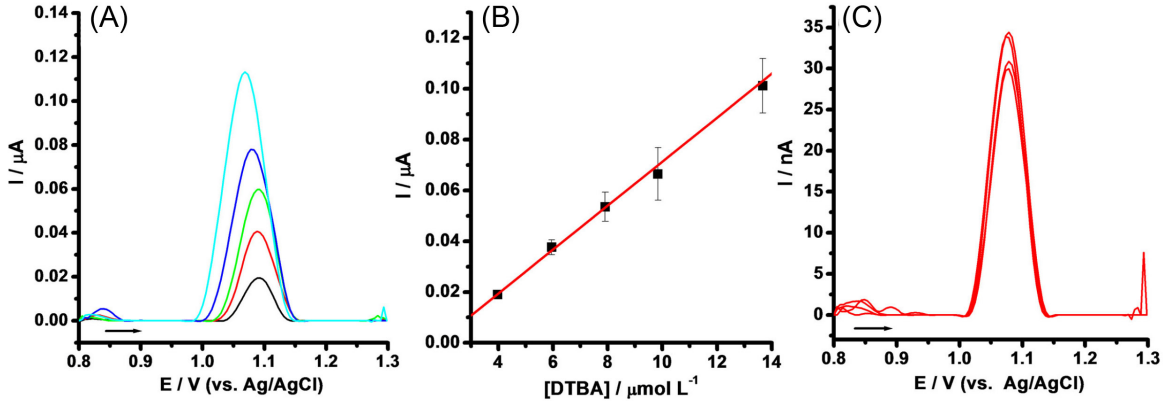

Figure 7. (A) DPVs on GCE (3.0 mm) obtained in DTBA solution at increasing concentrations. (B) Analytical curve I_{pa} (A) = 0.008(DTBA / (μmol L^{-1})) – 1.33 × 10^{-8}. [Phosphate buffer] = 0.1 mol L^{-1}, pH = 7.0; (a) 3.98, (b) 5.95, (c) 7.91, (d) 9.84, (e) 13.67 μmol L^{-1}. Error bars represent the standard deviation for three independent measurements. (C) Repeatability study (n = 4) using a 6 μmol L^{-1} DTBA solution.

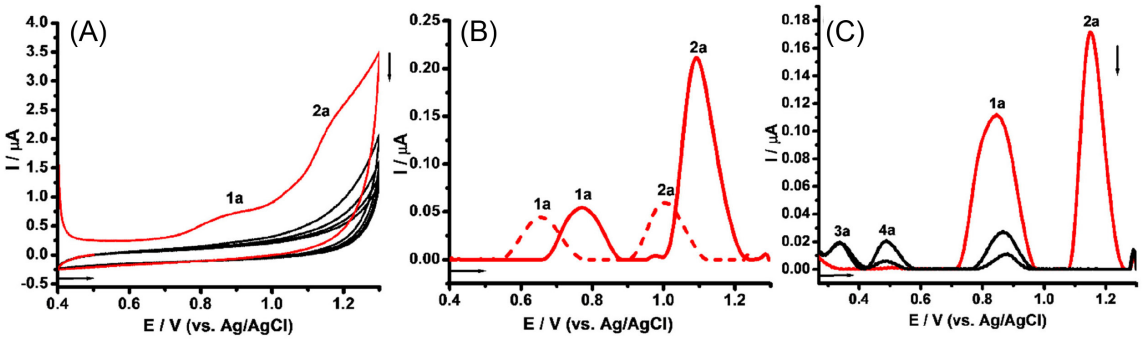

Figure 8. ATZ thin film on GCE (1.6 mm): (A) Consecutive cyclic voltammograms in acetate buffer (pH = 4.5), (B) DPVs in acetate buffer (pH = 4.5) (—) and in phosphate buffer (pH = 7.0) (---) and (C) successive SWVs in acetate buffer (pH = 4.5). (—) First scan.

The CV experiments were repeated using DPV. DPVs of the ATZ thin film on the GCE, in acetate buffer, at pH = 4.5, showed two subsequent anodic peaks at E_{p1a} = 0.77 V and E_{p2a} = 1.09 V. In the physiological neutral medium, their potentials were shifted, as expected, for lower positive values, at E_{p1a} = 0.65 and E_{p2a} = 1.00 V, Figure 8B, indicating the deprotonation of the electroactive amino acids involved.[29,36-38]

Thus, in a more extended potential window, successive SWVs of the ATZ monolayer thin film were recorded in acetate buffer, pH = 4.5, Figure 8C. In the first SWV scan of the ATZ, Figure 8C, two oxidation peaks (E_{p1a} = 0.84, E_{p2a} = 1.15 V) were observed in agreement with DPV and CV, Figures 8A and 8B. In the second scan, recorded under the same experimental conditions without cleaning the GCE surface, two new anodic processes were identified, peak 3a (E_{p3a} = 0.33 V) and peak 4a (E_{p4a} = 0.48 V), and were associated with electroactive ATZ oxidation products.

The electrochemical response of proteins on solid electrode surfaces was initially associated only with the primary structure and consequently with electroactive amino acid residues.[24,25,36-38] Recent studies,[24,25,36-38] however, have associated a strong influence of the tertiary and quaternary structures of these species. These studies indicate that only outwardly oriented amino acids will be on the electrode surface available for electrochemical reactions.[24,25,36-38]

The electro-oxidation of Trp and Tyr in neutral medium, phosphate buffer, on GCE were revisited by voltammetric and EIS techniques, Figures 9 and 10 and Table 2, and compared with data from ATZ, Figure 8 and Table 2.

Consecutive cyclic and DPVs were recorded in the 1.0 mmol L^{-1} Trp aqueous solution (pH = 7.0), Figures 9A and 9B. The cyclic voltammograms of Trp, Figure 9A and Table 2, detected two subsequent irreversible anodic peaks, peak 1a at E_{p1a} = +0.81 V and peak 2a at E_{p2a} = +1.12 V.[31,32] From the consecutive scans, the CV data also identified a very significant decrease in peak 1a current and the disappearance of process 2a, Figure 9A. New CV experiments were carried out, confirming strong adsorption of Trp oxidation products on the GCE, since, as shown in Figure 9A, the initial Trp voltammetric response was not recovered by rinsing the electrode surface. On the other hand, in the first potential scan, the DPVs detected peak 1a at E_{p1a} = +0.68 V; I_{p1a} = 3.14 µA and peak 2a at E_{p2a} = +1.08 V; I_{p2a} = 0.16 µA,[32] Figure 9B and Table 2. From the second potential scan, two new processes were easily observed, peak 3a at E_{p3a} = +0.07 V and peak 4a at E_{p4a} = +0.35 V.[32]

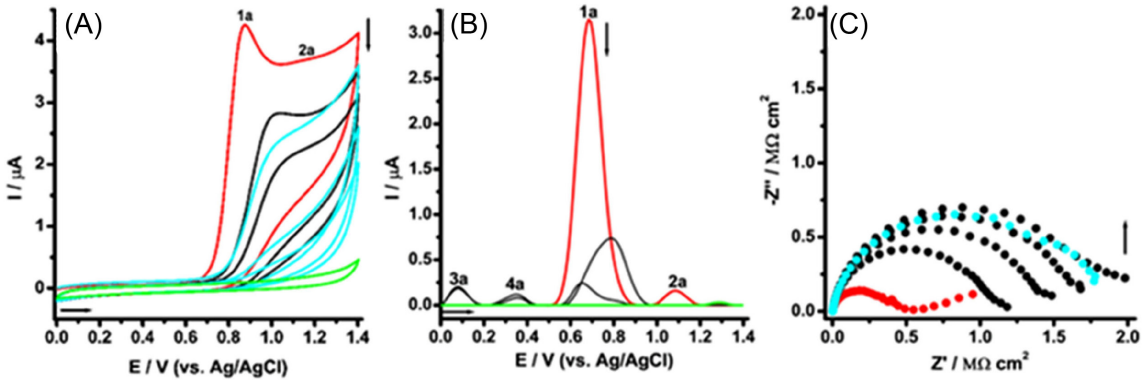

Figure 9. Consecutive scans on GCE (1.6 mm) in 1.0 mmol L^{-1} Trp in phosphate buffer (pH = 7.0). First scan (—), consecutive scans after washing the GCE (—) and the supporting electrolyte (—). (A) CV, (B) DPV and (C) EIS at E_{ap} = + 0.80 V.

Table 2. Peak potentials of Trp, Tyr and Cys in phosphate buffer (pH = 7.0) in CV and DPV on GCE

Species	Peak potentials (E / V *vs.* Ag/AgCl)							
	CV				DPV			
	Peak 1a / V	Peak 2a / V	Peak 3a / V	Peak 4a / V	Peak 1a / V	Peak 2a / V	Peak 3a / V	Peak 4a / V
Trp	+0.81	+1.12	–	–	+0.68	+1.08	+0.07	+0.35
Tyr	+0.74	–	–	–	+0.64	–	–	–
ATZ	–	–	–	–	+0.65	+1.00	–	–

CV: cyclic voltammetry; DPV: differential pulse voltammetry; Trp: tryptophan; Tyr: tyrosine; ATZ: alemtuzumab.

EIS experiments offer an excellent way to further investigate the phenomenon of adsorption.[34,35] Given this, consecutive EI spectra were recorded, at E_{ap} = +0.80 V, in a 1.0 mmol L^{-1} Trp solution (pH = 7.0). The first EI spectrum of Trp, Figure 9C, detected a semicircle, at high frequencies, due to the charge-transfer reaction, as well as a straight line at a low frequency range, associated with a diffusion-limited oxidation process.[34,35] From the second EI spectra, a significant increase in the semicircle portion is clearly observed, Figure 9C, as well as the fact that the response of the GCE has not recovered after its surface was rinsed with water, Figure 9C.

All EI spectra, Figure 9C, were fitted adequately by the Randles circuit,[34] that includes the ohmic resistance of the electrolyte solution (R_Ω), the constant phase element (CPE), the charge transfer resistance (R_{ct}) and the Warburg impedance (ZW) resulting from the diffusion of Trp from the bulk solution to the GCE surface.[34] The diameter of the semicircle is a measure of the R_{ct} and was observed that R_{ct} increases by the successive EI spectra, confirming the adsorption of Trp oxidation products on GCE surface, Table 3.

For the Tyr study, a 1.0 mmol L^{-1} Tyr solution prepared in phosphate buffer was used. Consecutive cyclic voltammograms were recorded, Figure 10A, and identified a single irreversible peak 1a at E_{p1a} = +0.74 V.[22,30] The results from these consecutive scans also demonstrated a significant decrease in peak 1a current, both before and after washing the electrode surface with ultrapure water, Figure 10A. The DPVs of Tyr, Figure 10B and Table 2, also identified only a single anodic peak, 1a, in the first scan, at E_{p1a} = +0.64 V and I_{p1a} = 7.52 µA.[22,30] In the second scan, however, peak 1a was detected at E_{p1a} = +0.73 V and with I_{p1a} = 2.06 µA. These voltammetric results indicate that Tyr oxidation product(s) adsorb on GCE, passivating its surface and hindering subsequent redox processes.[22,30]

Six consecutive EIS readings were then recorded in a 1.0 mmol L^{-1} Tyr solution at pH = 7.0, applying a fixed

Table 3. Fitting parameters of the impedance data for 1.0 mmol L^{-1} Trp and Tyr in phosphate buffer (pH = 7.0), on GCE surface

Species	Values of R_{ct} / (MΩ cm^2)						
	1st scan	2nd scan	3rd scan	4th scan	5th scan	6th scan	7th scan
Trp (at 0.80 V)	0.37	1.03	1.36	1.58	1.78	1.67[a]	–
Tyr (at 0.65 V)	0.14	0.24	0.28	0.32	0.37	0.42	0.39[a]

[a]Consecutive scans after washing the GCE; Trp: tryptophan; Tyr: tyrosine; R_{ct}: charge transfer resistance.

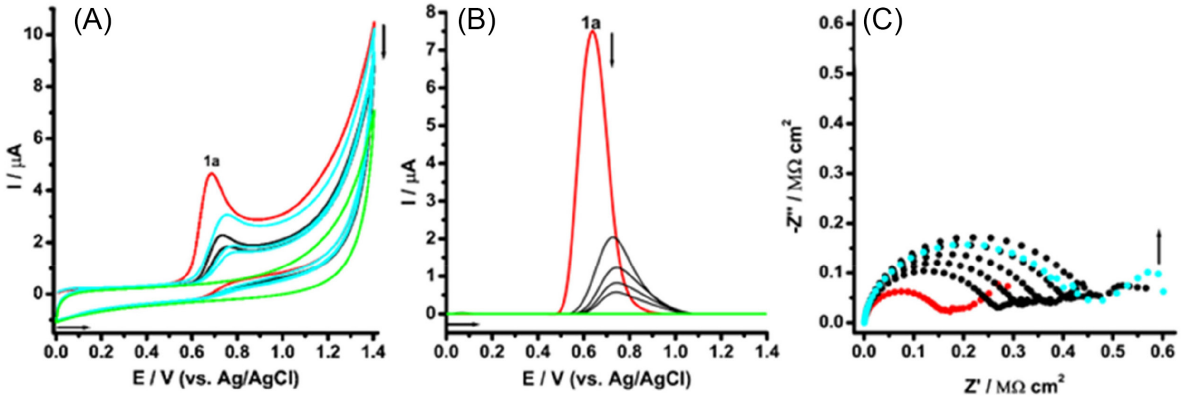

Figure 10. Consecutive scans on GCE (1.6 mm) in 1.0 mmol L^{-1} Tyr in phosphate buffer (pH = 7.0). First scan (—), consecutive scans after washing the GCE (—) and the supporting electrolyte (—). (A) CV, (B) DPV and (C) EIS at E_{ap} = + 0.65 V.

potential of E_{ap} = + 0.65 V, Figure 10. An increase in the radius of the semicircle of the Tyr spectra shown in Figure 10C was observed, indicating a greater resistance of the GCE arising from the redox reactions that occur on its surface, Table 3. Before the seventh reading, the electrode was washed and the solution was homogenized. The recorded spectrum also showed a high resistance in relation to the first scan, Figure 10C and Table 3. These data from EIS, Figure 10C, confirm the voltammetric results, Figures 10A and 10B, and indicate that the electro-oxidation products of Tyr are able to form a resistive film that is strongly adsorbed on the electrode, requiring mechanical cleaning for its removal.

From the ATZ voltammetric data, Figure 8, Trp, Figure 9, and Tyr, Figure 10, Table 2 and previous data,[29,36-38] it was possible to conclude that the oxidation of ATZ on GCE occurs in two subsequent irreversible and pH-dependent steps. The first step was related to the electro-oxidation of outward-oriented Trp and Tyr residues that were in direct contact with the electrode surface. The second step occurred due to the second step of oxidation of Trp residues, with the formation of two electroactive products (quinone derivatives).

These voltammetric results were important and demonstrated potential, mainly of pulse techniques (DPV and SWV) for the detection and quantification of electroactive protein residues, as well as their oxidation products with high selectivity and sensitivity on the GCE surface. A future proposal, considering the results here and data from previous reports in the literature,[29,36-38] would be to further investigate the electro-oxidation of ATZ after the action of a reducing/denaturing agent, DTBA and/or DTT.

Conclusions

The voltammetric study demonstrated that DTBA protein denaturing agents as well as DTT are both susceptible to direct electro-oxidation on GCE. The oxidation of DTBA is controlled predominantly by diffusional mass transport and occurs in three subsequent irreversible pH-dependent steps. The first two steps are electro-oxidations of the thiol groups, with the removal of two electrons and two protons, forming a cyclic intermediate by the disulfide bond. The electrochemical results presented here also indicated differences in relation to the anodic behavior between the denaturants, since the first anodic process was always observed for DTBA, but not for DTT, and the peak 2a' was detectable only in DTT. The DTBA and DTT oxidation mechanisms are thus postulated and proposed.

An electroanalytical method for DTBA has been established using DPV at GCE in physiological medium with a LOD of 0.61 μmol L^{-1} and LOQ of 2.05 μmol L^{-1}.

The anodic behavior of the monoclonal antibody ATZ on GCE was also characterized and established using voltammetric techniques. The results using DPV and SWV pulse techniques clearly demonstrated the spontaneous adsorption of ATZ on the hydrophobic surface of the GCE and that ATZ undergoes electro-oxidation in two subsequent irreversible steps, both pH-dependent, with formation of two electroactive products. The oxidation processes of ATZ were related to its superficially exposed Trp and Tyr amino acid residues on the three-dimensional structure of the protein and on the GCE surface. An oxidation mechanism of ATZ is then proposed.

Knowing the redox mechanism of DTBA, DTT and the antineoplastic agent ATZ on a GCE will possibly be useful in the field of molecular biochemistry. These studies may also clarify mechanisms related to redox stability, physiological and pharmacological activity of these investigated species.

Acknowledgments

Financial support from Fundação de Amparo à Ciência e Tecnologia do Estado de Pernambuco (FACEPE), PPP/FACEPE/CNPq/APQ-0535-1.06/14, Conselho Nacional de Desenvolvimento Científico e Tecnológico (CNPq), MCTI/CNPQ/Universal/APQ-422757/2018-7, PhD Student - FACEPE grant (N. L. Queiroz and M. L. Nascimento), CAPES PhD Grant 88887.483445/2020-00 (J.A.M. Nascimento) and PIBIC-CNPq-UFRPE Grant (M.W.F. Silva and J.G.S. Neto) are gratefully acknowledged.

Author Contributions

Nathalia L. Queiroz was responsible for investigation, methodology, analysis and writing; Maycom W.F. Silva for investigation, methodology and analysis; Maysa L. Nascimento for investigation, methodology and analysis; José G. da Silva Neto for investigation and analysis; José Ailton M. Nascimento for investigation, methodology and analysis; Katia C.S. Freitas for methodology and investigation, Eric S. Gil for methodology and investigation and Severino Carlos B. Oliveira for project coordinator, methodology, analysis, investigation, writing review and editing.

References

1. Lukesh, J. C.; Palte, M. J.; Raines, R. T.; *J. Am. Chem. Soc.* **2012**, *134*, 4057. [Crossref]
2. Santarino, I. B.; Oliveira, S. C. B.; Oliveira-Brett, A. M.; *Electrochem. Commun*. **2012**, *23*, 114. [Crossref]

3. Lamoureux, G. V.; Whitesides, G. M.; *J. Org. Chem*. **1993**, *58*, 633. [Crossref]
4. Dunaway-Mariano, D.; Holden, H. M.; Raushel, F. M.; *Biochemistry* **2013**, *52*, 9092. [Crossref]
5. Cline, D. J.; Redding, S. E.; Brohawn, S. G.; Psathas, J. N.; Schneider, J. P.; Thorpe, C.; *Biochemistry* **2004**, *43*, 15195. [Crossref]
6. Adamczyk, J.; Bal, W.; Krężel, A.; *Inorg. Chem.* **2015**, *54*, 596. [Crossref]
7. Le Basle, Y.; Chennell, P.; Tokhadze, N.; Astier, A.; Sautou, V.; *J. Pharm. Sci.* **2020**, *109*, 169. [Crossref]
8. Teo, E. C.; Chew, Y.; Phippis, C.; *Crit. Rev. Oncol./Hematol*. **2016**, *97*, 72. [Crossref]
9. Zahavi, D.; Weiner, L.; *Antibodies* **2020**, *9*, 34. [Crossref]
10. Di Ioia, M.; Di Stefano, V.; Farina, D.; Di Tommaso, V.; Travaglini, D.; Pietrolongo, E.; Sensi, S. L.; Onofrj, M.; De Luca, G.; *Mult. Scler. Relat. Disord.* **2020**, *38*, 101504. [Crossref]
11. Isaacs, J. D.; Hale, G.; Cobbold, S. P.; Waldmann, H.; Watts, R. A.; Hazleman, B. L.; Keogan, M. T.; *Lancet* **1992**, *340*, 748. [Crossref]
12. Vital, E. M.; Emery, P.; *J. Autoimmun.* **2008**, *31*, 219. [Crossref]
13. Lockwood, C. M.; Thiru, S.; Isaacs, J. D.; Hale, G.; Waldmann, H.; *Lancet* **1993**, *341*, 1620. [Crossref]
14. Díaz-Orta, M. A.; Rojas-Serrano, J.; *Reumatol. Clin*. **2011**, *7*, 33. [Crossref]
15. Isaacs, J. D.; Hazleman, B. L.; Chakravarty, K.; Grant, J. W.; Hale, G.; Waldmann, H.; *J. Rheumatol.* **1996**, *23*, 1103. [Link] accessed in November 2023
16. Alinari, L.; Lapalombella, R.; Andritsos, L.; Baiocchi, R. A.; Lin, T. S.; Byrd, J. C.; *Oncogene* **2007**, *26*, 3644. [Crossref]
17. Lovino, A.; Aruta, F.; Carotenuto, A.; Manganelli, F.; Iodice, R.; *Mult. Scler. Relat. Disord.* **2019**, *28*, 98. [Crossref]
18. Chirikov, V.; Ma, I.; Joshi, N.; Patel, D.; Smith, A.; Giambrone, C.; Cornelio, N.; Hashemi, L.; *Value Health* **2019**, *22*, 168. [Crossref]
19. Notas, K.; Papadaki, E.; Orologas, A.; Moschou, M.; Kimiskidis, V. K.; *Scler. Relat. Disord*. **2020**, *38*, 101517. [Crossref]
20. Chiorcea-Paquim, A. M.; Oliveira-Brett, A. M.; *J. Pharm. Biomed. Anal.* **2023**, *222*, 115036. [Crossref]
21. Chiorcea-Paquim, A. M.; Enache, T. A.; Gil, E. S.; Oliveira-Brett, A. M.; *Compr. Ver. Food Sci. Food Saf.* **2020**, *19*, 1680. [Crossref]
22. Nascimento, M. L.; Alves, A. S.; Nascimento, J. A. M.; Santos, V. B.; Oliveira, S. C. B.; *Carbon Trends* **2022**, *8*, 100182. [Crossref]
23. Budak, F.; Cetinkaya, A.; Kaya, S. I.; Atici, E. B.; Ozkan, S. A.; *Diamond Relat. Mater.* **2023**, *133*, 109751. [Crossref]
24. Oliveira-Brett, A. M.; Diculescu, V. C.; Enache, T. A.; Fernandes, I. P. G.; Chiorcea-Paquim, A. M.; Oliveira, S. C. B.; *Curr. Opin. Electrochem.* **2019**, *14*, 173. [Crossref]
25. Suprun, E. V.; *Electrochem. Commun.* **2021**, *125*, 106983. [Crossref]
26. da Costa, J. G. R.; Costa, J. M.; Almeida Neto, A. F.; *J. Environ. Chem. Eng.* **2021**, *9*, 106355. [Crossref]
27. Kalinke, C.; Oliveira, P. R.; Banks, C. E.; Janegitz, B. C.; Bonacin, J. A.; *Sens. Actuators, B* **2023**, *381*, 133353. [Crossref]
28. Bandodkar, A. J.; Wang, J.; *Trends Biotechnol.* **2014**, *32*, 363. [Crossref]
29. Oliveira, S. C. B.; Santarino, I. B.; Oliveira-Brett, A. M.; *Electroanalysis* **2013**, *25*, 1029. [Crossref]
30. Nascimento, R. F.; Nascimento, M. L.; Nascimento, J. A. M.; Santos, H. N. L.; Araújo, A. P.; Oliveira, S. C. B.; *J. Electroanal. Chem.* **2019**, *854*, 113535. [Crossref]
31. Enache, T. A.; Oliveira-Brett, A. M.; *Electroanalysis* **2011**, *23*, 1337. [Crossref]
32. Queiroz, N. L.; Mendes, C. H. S.; Nascimento, J. A. M.; Silva, M. W. F.; Oliveira, J. E. S.; Oliveira, S. C. B.; *Electroanalysis* **2023**, *35*, e202200249. [Crossref]
33. Enache, T. A.; Oliveira-Brett, A. M.; *Bioelectrochemistry* **2011**, *81*, 46. [Crossref]
34. Brett, C. M. A.; Oliveira-Brett, A. M.; *Electrochemistry: Principles, Methods and Aplications*; Oxford Science University Publications ed.: Oxford, UK, 1993.
35. Wang, J.; *Analytical Electrochemistry*, 3rd ed.; Wiley: New York, USA, 2006.
36. Safavi, A.; Ahmadi, R.; Mahyari, F. A.; *Amino Acids* **2014**, *46*, 1079. [Crossref]
37. Issaad, F. Z.; Tomé, L. I. N.; Marques, N. V.; Mouats, C.; Diculescu, V. C.; Oliveira-Brett, A. M.; *Electrochim. Acta* **2016**, *206*, 246. [Crossref]
38. Machini, W. B. S.; Marques, N. V.; Oliveira-Brett, A. M.; *J. Electroanal. Chem.* **2019**, *851*, 113251. [Crossref]

Submitted: July 27, 2023
Published online: November 30, 2023